POLSKA AKADEMIA NAUK

INSTYTUT MASZYN PRZEPŁYWOWYCH

PRACE INSTYTUTU MASZYN PRZEPŁYWOWYCH

TRANSACTIONS

OF THE INSTITUTE OF FLUID-FLOW MACHINERY

92

WARSZAWA—POZNAŃ 1990

PAŃSTWOWE WYDAWNICTWO NAUKOWE

PRACE INSTYTUTU MASZYN PRZEPŁYWOWYCH

poświęcone są publikacjom naukowym z zakresu teorii i badań doświadczalnych w dziedzinie mechaniki i termodynamiki przepływów, ze szczególnym uwzględnieniem problematyki maszyn przepływowych

*

THE TRANSACTIONS OF THE INSTITUTE OF FLUID-FLOW MACHINERY

exist for the publication of theoretical and experimental investigations of all aspects of the mechanics and thermodynamics of fluid-flow with special reference to fluid-flow machinery

REDAKCJA–EDITORIAL OFFICE

Instytut Maszyn Przepływowych PAN
ul. Gen. Józefa Fiszera 14, 80-952 Gdańsk, skr. pocztowa 621, tel. 41-12-71

Printed in Poland

ISBN 83-01-10189-X
ISSN 0079-3205

PAŃSTWOWE WYDAWNICTWO NAUKOWE — ODDZIAŁ W POZNANIU

Ark. wyd. 17,75. Ark. druk. 13. Papier druk. sat. kl. III, 70 g, 70 × 100 cm
Oddano do składania w lipcu 1989 r. Podpisano do druku w listopadzie 1990 r.
Druk ukończono w grudniu 1990 r. Zam. nr 1079/89

Zakłady Graficzne im. KEN w Bydgoszczy

PRACE INSTYTUTU MASZYN PRZEPŁYWOWYCH
1990 Zeszyt 92

MANFRED HACKESCHMIDT, HANS-DIETER HILBRICH
MATHIAS RÖSSLER, NORBERT KRÜGER

Dresden*)

Secondary Flows in Curved Channels of Arbitrary Cross Section Variation**)

In order to calculate energy losses caused by secondary flows in curved channels of any sectional change a mathematical model of a stationary, inviscid (ideal) flow field has been applied. The qualitative correspondence between the wall streamlines in a specially curved channel determined numerically (FORTRAN program) and the wall streamlines displayed experimentally in a wind channel has led to the development of a calculation method for three-dimensional boundary layers. Fundamental results of the behaviour of secondary flows due to different effects are given in the present paper.

1. Statement of the Problem

As it is well-known, flows along curved channels are of a typical three-dimensional nature, and their energy loss calculation is generally based on empirical-heuristic correlations found experimentally. It is evident from Fig. 1 that the total pressure boundary loss coefficient of plane blade cascades — passed through without separation — can be assessed from the empirical relationship

$$\zeta_r = 1.43 \cdot 10^{-2} f(\delta_1^*) + 2 \cdot 10^{-4} (\beta_1 - \beta_2) \frac{\sin\beta_2}{\sin\beta_1} (1 \pm 0.1)$$

The main influential parameters are the inflow and outflow angles, β_1 and β_2, according to the structure found by H. Wolf [13]***) and the displacement thickness,

*) Friedrich List University of Transport and Communications, Department of Vehicle Engineering, Dresden, German Democratic Republic.

**) Paper read by M. Rössler on October 25, 1984, at the Technical University of Gdańsk as an extended version of a publication to the „Hydrosoft" Conference in Portorož, Yugoslavia, September 10—14, 1984, copyright by CML Publications, Ashurst Lodge, Ashurst, Southampton SO42AA, England.

***) It should be noticed that the β_1 and β_2 values appearing in Fig. 1 and the above equation are expressed in grades (grd) and not angle degrees (°). In general

$\frac{\sin\beta_2}{\sin\beta_1}$ > 1 in case of decelerated flow,
$= 1$ in case of „equal pressure" flow,
< 1 in case of accelerated flow.

When a higher degree of accuracy is required it must be taken into account that the functional dependence on the factor $\sin\beta_2/\sin\beta_1$ increases in a slightly progressive way.

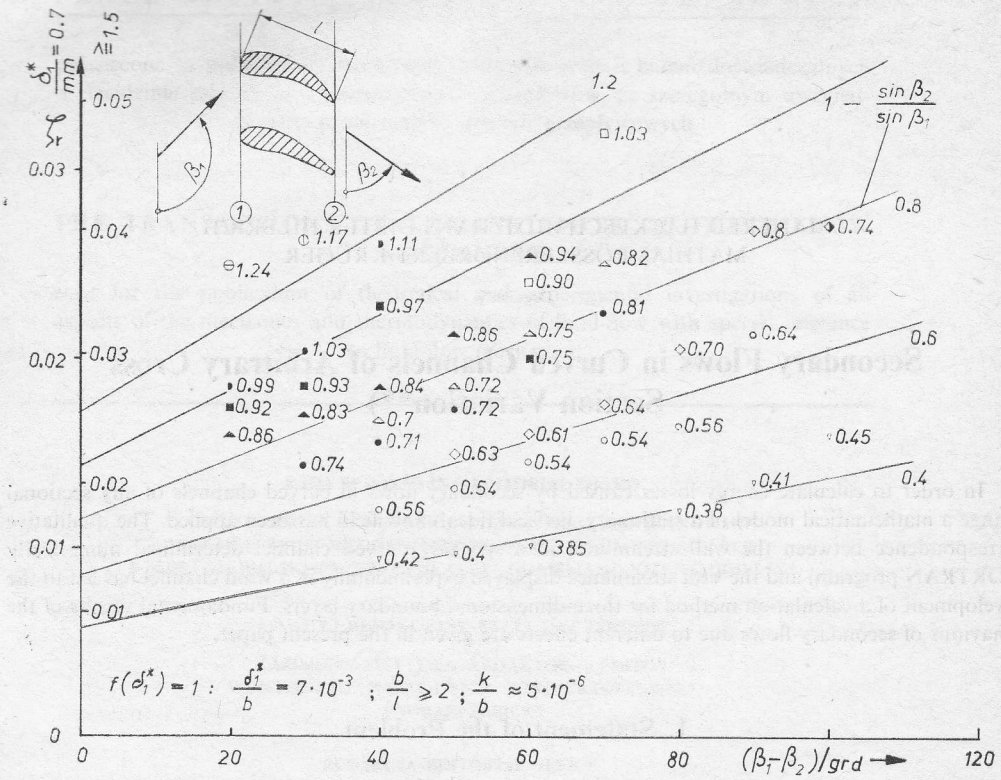

Fig. 1. Empirical correlation of the total pressure boundary loss coefficient ζ_r and the following quatities: β_1 — cascade inlet angle, β_2 — cascade outlet angle, δ_1^* — displacement thickness on the channel side wall in the cascade inlet plane ① (measuring points fixed by H. Wolf [13] for the parameters at lower left corner of the figure and valid for a small turbulence degree at the exit), b — channel height (perpendicular to the figure plane), l — profile chord length, k — peak-to-valley height of channel surfaces
The right ordinate scale applies to the re valuation recommendation according to [6]. The pressure losses shown in Fig. 1 are related to the dynamic pressure in the cascade inlet plane ① in case of decelerated flow, in all the other cases to that in the cascade outlet plane ②

δ_1^*, in the cascade inlet plane for which M. Hultsch and H. Sauer [6] recommended a re-valuation (see the scale at the right hand side of the ordinate axis in Fig. 1). A dependence of this inlet displacement thickness on other relevant influential parameters is unknown.

Due to a number of further parameters being of importance, including velocity, vorticity and turbulence degree distributions, observed in channel inlet sections, sectional path of curved channels, longitudinal vortex in the corner, separation areas and so on, loss calculation is possible only in a relatively rough way (evaluation) or else an adequately large number of information must be given.

An alternative to this is to use a mathematical model allowing for the sufficiently exact calculation of secondary flows in curved channels of any sectional change which run in the main flow direction. By means of this model it is possible to analyse

the three-dimensional flow field in order to develop efficient installations serving to influence the secondary flow field. In this way a possibility is seen for designing arbitrarily curved channels of any shape with power limiting properties.

2. The Mathematical Model

A clear explanation for the formation of secondary flows was given by E. Lindner [8]. The mechanism of vortex formation is based on the existence of a side wall boundary layer of transversal velocity distribution $v_\varepsilon(z)$ in the inlet plane ① of the curved channel as demonstrated in Fig. 2. Due to the pressure difference between the suction side *SS* and the pressure side *PS* this boundary layer is more strongly deflected than the basic flow in the curved channel. Some basic relationships governing fluid rotation are given in Table 1. Although the secondary flow is caused by a friction effect, its development in the curved channel may be considered by means of a friction-free model, i.e. that of an ideal fluid. This model results in the Helmholtz vortex equation (1) shown in Table 2. By simplification, the equation system (3) is obtained if the basic flow velocity distribution $v_\varepsilon(r)$ in the curved channel of constant cross-section is approximated according to the law (2) of the free vortex (see Appendix). Equation (3.2) describes the Helmholtz vortex theorem according to which the circulation (1) (see Table 1) of a vortex filament shown in Fig. 2 remains constant with time.

Using the relationship (2) in Table 2 it is possible to differentiate the right side of equation (3.1), and thus the common differential equation (4) and its integral (5) are obtained. The above integral represents a change of the peripheral component of rotation ω_ε in the curved channel of constant cross-section, being proportional to the angle of curvature ε. This law can be explained by means of another Helmholtz vortex theorem (2) shown in Table 1 and stating that vortex tubes consist permanently of the same fluid volume. This volume moves with the basic flow velocity $v_\varepsilon(r)$, i.e. more slowly at the pressure side *PS* than at the suction side *SS*. This means that in the present case the rotation vector ω moves with double angular velocity in

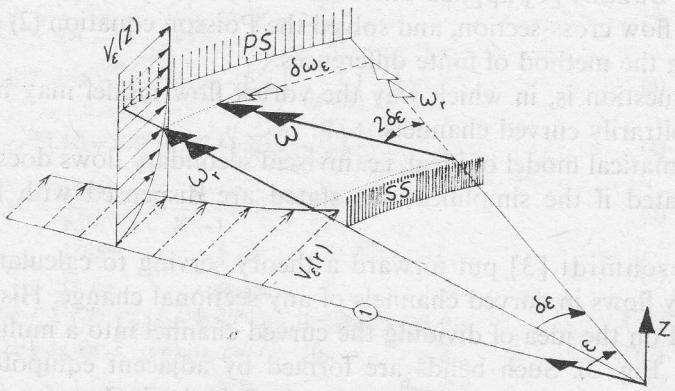

Fig. 2. Schematic diagram of fluid rotation in the curved channel of constant cross-section

Table 1
Basic assumptions on fluid rotation in the curved channel of constant cross-section (Fig. 2)

$\delta\Gamma = \omega\delta A$	(1)
$\delta V = \text{const}$	(2)
$\omega_r = \frac{\partial v_\varepsilon}{\partial z}$	(3)

Table 2
Mathematical model of an ideal secondary flow in a plane curved channel of constant cross-section

$(\vec{v}\nabla)\vec{\omega} = (\vec{\omega}\nabla)\vec{v}$	(1)
$v_\varepsilon r = \text{const}$	(2)
$\frac{v_\varepsilon}{r^2}\frac{\partial\omega_\varepsilon}{\partial\varepsilon} = \omega_r\frac{\partial}{\partial r}\left(\frac{v_\varepsilon}{r}\right)$	(3.1)
$\omega_r = \text{const}$	(3.2)
$\omega_z = 0$	(3.3)
$\frac{d\omega_\varepsilon}{d\varepsilon} = -2\omega_r$	(4)
$\delta\omega_\varepsilon = -2\delta\varepsilon\cdot\omega_r$	(5)

direction opposite to that of the homologous elementary fluid volume of the basic flow (see Fig. 2).

Theoretical investigations of secondary flows based on the Helmholtz vortex equation (1) (see Table 2) were made by H. B. Squire and K. G. Winter [12]. They restricted their studies to bends of invariably rectangular cross-section being very flat in the meridional plane, i.e. of high aspect ratio $\Delta z/\Delta n$. In such a case it is possible to determine analytically the stream function of the quasi-plane secondary flow field on the basis of the fundamental result saying that the vortex of the secondary flow in the persistent basic flow, i.e. in the bend of constant cross-section $\Delta z\cdot\Delta r$, is proportional to the bend angle $\Delta\varepsilon$ and the axial velocity gradient of the actual basic flow upstream of the cascade (see equation (2) in Table 3).

R. Puzyrewski [10] modified the model of the ideal secondary flow by replacing the coefficient $\Phi = 2\Delta\varepsilon$ in Eq. (5) of Table 2 by a function of the spanwise coordinate. He follows the vortex lines in the bend and points out that the coefficient Φ represents the cotangent of the angle formed between the vortex lines and the basic flow streamlines.

L. Bělík [2] modified the shape of the inflow velocity profile and the aspect ratio of the bend and showed their influence on the secondary flow field.

As the aspect ratio is comparatively high, the solution may be obtained analytically.

In 1975 D. Bažant [1] applied this vortex flow theory to bends of non-flat, but still invariable flow cross-section, and solved the Poisson equation (2) of Table 3 numerically using the method of finite differences.

Now the question is, in which way the vortex flow model may be modified to apply it to arbitrarily curved channels.

The mathematical model of ideal, i.e. inviscid secondary flows does not get much more complicated if the simplifications stated are dispensed with from the very beginning.

M. Hackeschmidt [3] put forward a theory serving to calculate ideal stationary secondary flows in curved channels of any sectional change. His mathematical model is based on the idea of dividing the curved channel into a multitude of bends (partial knees, Fig. 3). Such bends are formed by adjacent equipotential surfaces (which R. Puzyrewski calls Bernoulli surfaces) of the basic flow, i.e. the flow which

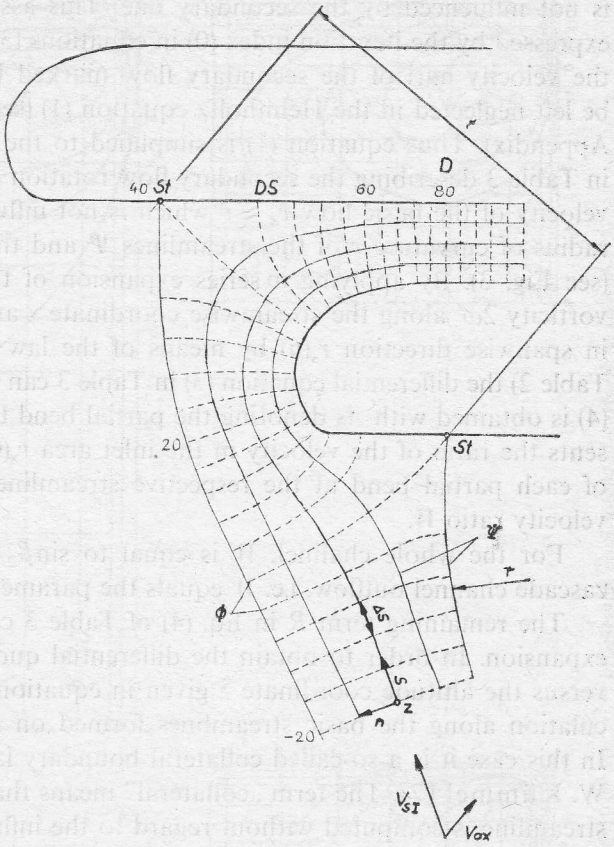

Fig. 3. The patterns of equipotential lines (Φ) and streamlines (Ψ) of the basic flow in the plane channel existing in the inlet range (i.e. without diffuser in the cascade channel outlet range); t — cascade pitch

Table 3

Mathematical model of an ideal secondary flow in a plane curved channel of arbitrarily variable cross-section

$$(\vec{v}\nabla)\vec{\omega} = (\vec{\omega}\nabla)\vec{v} \tag{1}$$

$$v_z = \frac{\partial \Psi}{\partial n},\ v_r = -\frac{\partial \Psi}{\partial z},\ \nabla^2 \Psi = 2\varepsilon \frac{\partial v_{\varepsilon 1}}{\partial z} \tag{2}$$

$$\vec{v}^{\prime(\Phi)} = \Phi,\ \frac{d(\omega^{\prime(\Phi)}/v_s)}{d(s/r)} = -\left(\frac{r}{v_s}\right)^2 \frac{\partial v_s}{\partial z}\frac{\partial}{\partial n}\left(\frac{v_s}{r}\right) \tag{3}$$

$$\omega^{\prime(\Phi)}(\Delta s) = \omega^{\prime(\Phi)}(\Phi) W + \left(2f\frac{\partial v_s}{\partial z} + \frac{R}{2}\right)\frac{\Delta s}{r} \tag{4}$$

$$W = \frac{v_s(\Delta s)}{v_s(0)},\ f = \frac{W}{W-1}\ln W \tag{5}$$

$$v_z' = \frac{1}{\Delta s}\frac{\partial \Psi'}{\partial n},\ v_n' = -\frac{1}{\Delta s}\frac{\partial \Psi'}{\partial z} \tag{6}$$

$$\frac{\partial}{\partial z}\left(\frac{1}{\Delta s}\frac{\partial \Psi'}{\partial z}\right) + \frac{\partial}{\partial n}\left(\frac{1}{\Delta s}\frac{\partial \Psi'}{\partial n}\right) = \begin{cases} -2\omega^{\prime(\Phi)}, & z \leqslant \delta_{z\omega} \quad (7.1) \\ 0, & z > \delta_{z\omega} \quad (7.2) \end{cases}$$

$$\delta_{z\omega} \geqslant \delta_z \tag{8}$$

is not influenced by the secondary one. This assumption of such a basic flow — expressed by the iteration index (0) in equations (3) and (4) in Table 3 — means that the velocity curl of the secondary flow marked by an apostrophe (′) may at first be left neglected in the Helmholtz equation (1) (see left condition (3) in Table 3 and Appendix). Thus equation (1) is simplified to the common differential equation (3) in Table 3 describing the secondary flow rotation $\omega'^{(\Phi)} = \omega^{(\Phi)}$ depending on the local velocity of the basic flow $v_s \approx \tilde{v}$ which is not influenced by the secondary flow, the radius of curvature r of the streamlines Ψ and the curvilinear coordinates s and n (see Fig. 3). By applying a series expansion of the basic flow velocity v_s and the vorticity $2\omega'$ along the streamwise coordinate s and approximating the dependence in spanwise direction $v_s(n)$ by means of the law $v_s r = \text{const}$ (after equation (2) in Table 2) the differential equation (3) in Table 3 can be integrated. In this way equation (4) is obtained with Δs denoting the partial bend thickness. The parameter W represents the ratio of the velocity in the inlet area $v_s(0)$ to that in the outlet area $v_s(\Delta s)$ of each partial bend at the respective streamline Ψ while f is a function of this velocity ratio W.

For the whole channel, W is equal to $\sin\beta_2/\sin\beta_1$ in the case of a wake-free cascade channel outflow, i.e. W equals the parameter in the empirical formula for ζ_r.

The remaining term R in Eq. (4) of Table 3 covers higher order terms of series expansion. In order to obtain the differential quotient of the basic flow velocity v_s versus the altitude coordinate z given in equations (3) or (4), a boundary layer calculation along the basic streamlines formed on the channel side wall is required. In this case it is a so-called collateral boundary layer, as described, for instance, by W. Kümmel [7]. The term „collateral" means that the boundary layer along the Ψ streamline is computed without regard to the influence of the secondary flow.

As the radius of curvature r of basic streamlines Ψ in a channel having stagnation points St (Fig. 3) can become very small, M. Hackeschmidt [4] has introduced the secondary flow stream function Ψ' (see equations (6) in Table 3) being a generalization of the Stokes flow function.

It satisfies the linear partial differential equation (7) of the second order, the local secondary flow velocity being contained in its right side, i.e. in its inhomogeneous term (7.1). Expression (7.1) is valid for the area of the side wall vorticity boundary layer that is a wall area in which according to (4) the vorticity differs from zero. The thickness $\delta_{z\omega}$ of this vorticity boundary layer equals or is greater than the friction boundary layer thickness δ_z (see equation (8)) in which vorticity is generated according to the second term of the right side in equation (4). Beyond the vorticity boundary layer (7.2) there is no secondary flow vorticity but the secondary flow field does exist. Therefore the partial differential equation (7) gets homogeneous.

3. Numerical Tests of the Mathematical Model

As an investigation object a special cascade channel was used (Fig. 3). Deflection was observed in its inlet area where the flow was mainly accelerated, whereas in the outlet area, in the present case downstream from the potential surface $\Phi = 80$, a nearly

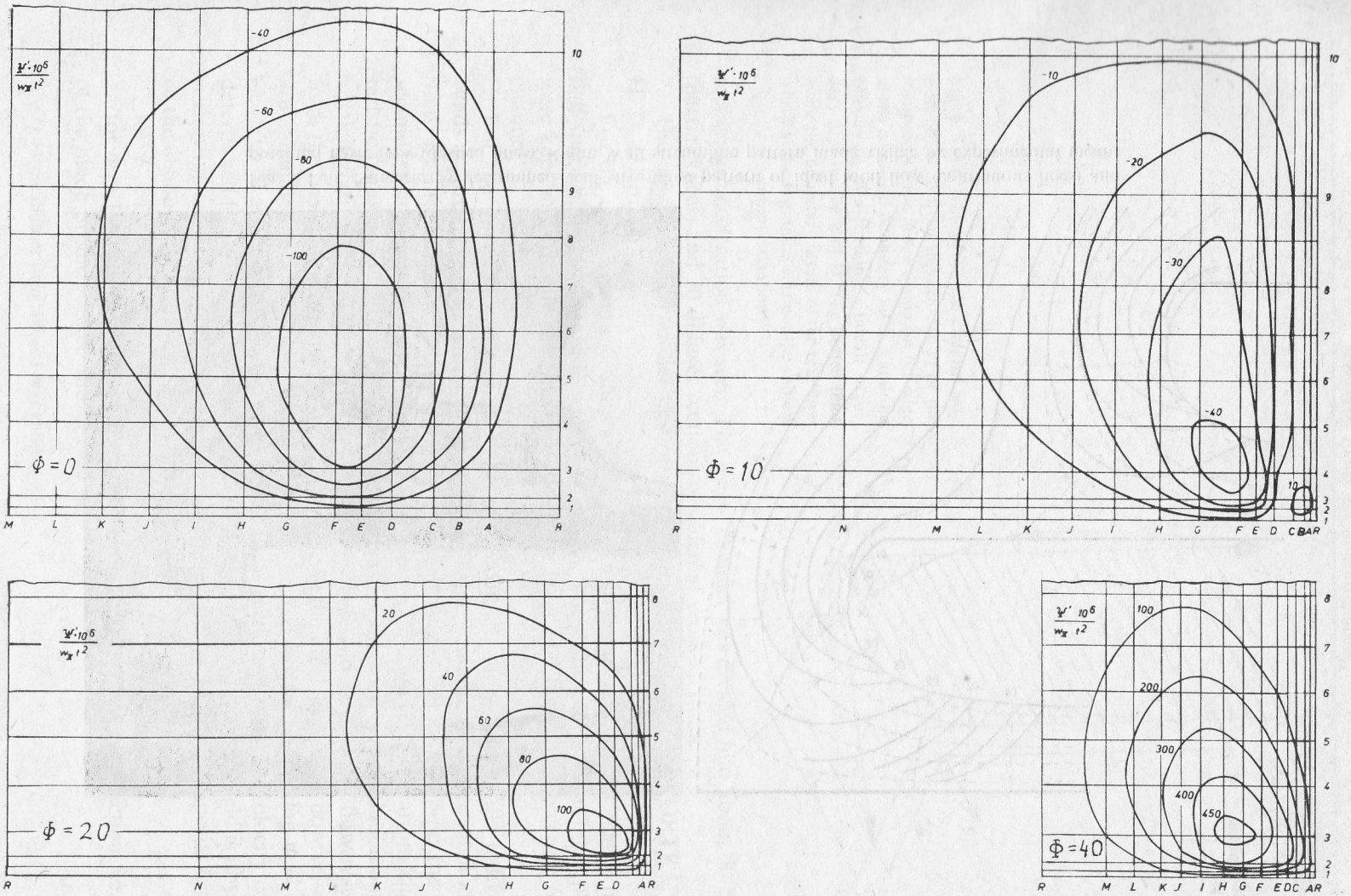

Fig. 4. Secondary flow stream function field $10^6 \Psi'/(v_{SS} \cdot t^2)$ in selected equipotential surfaces Φ (see Fig. 2)

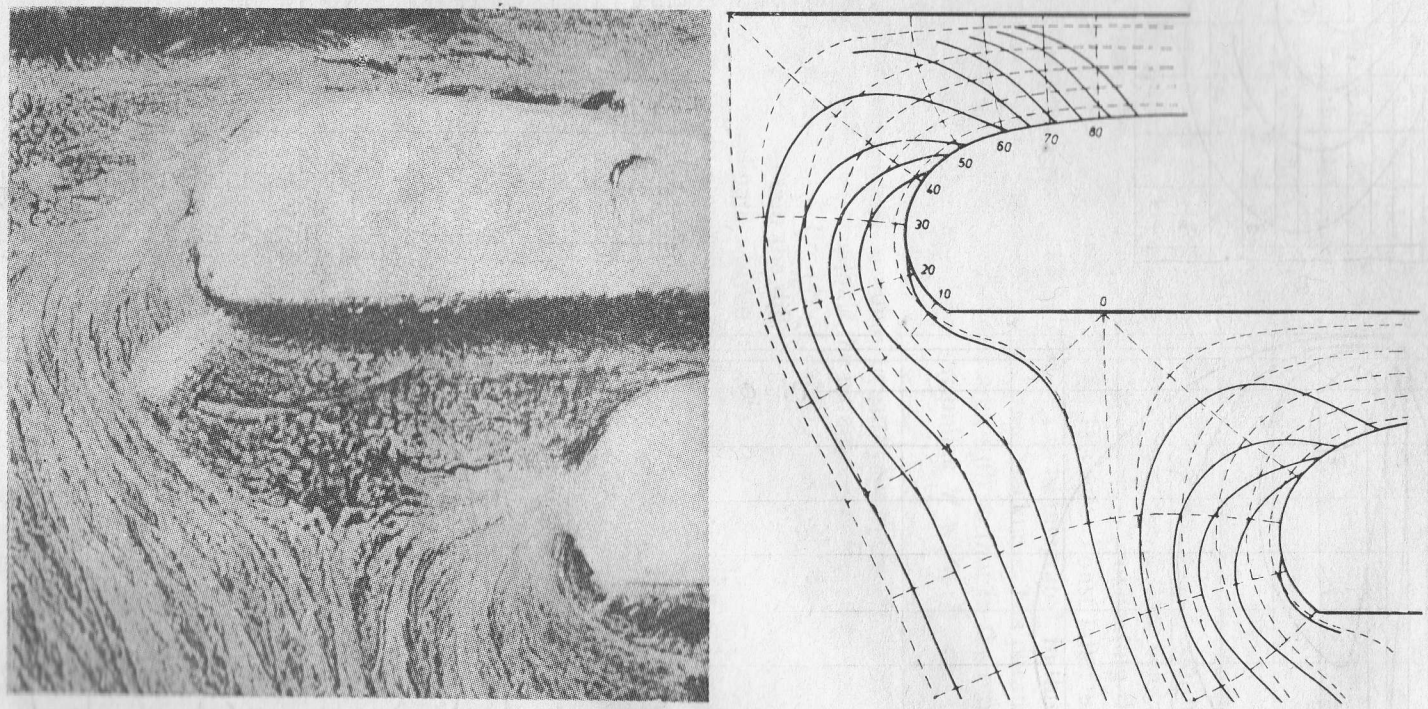

Fig. 5. Left: Numerically determined wall streamline pattern of ideal total flow (continuous lines) and potential basic flow (dashed lines). Right: Wall streamline pattern made visible by experimental means

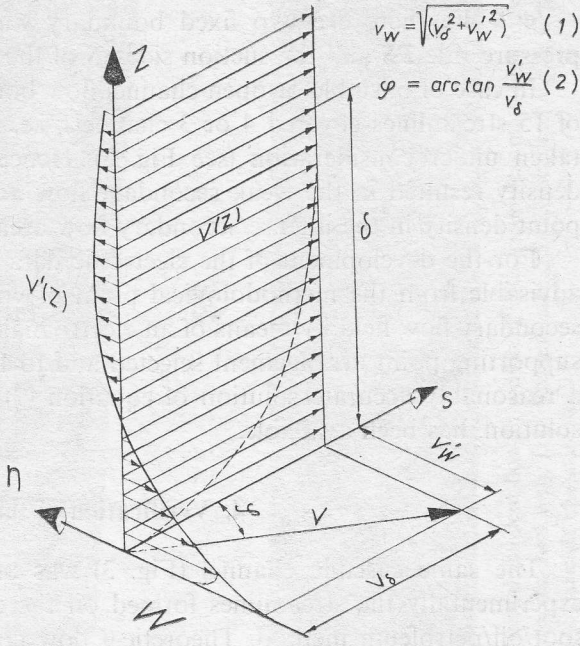

Fig. 6. Total velocity on the channel side wall obtained from the velocity v_δ of the frictionless basic flow existing on the edge of the collateral boundary layer δ and the velocity v'_W of a frictionless (ideal) secondary flow on the wall W. The dotted lines mark the boundary layers of the real flow which at the beginning was not the subject of investigation

rectilinear deceleration was seen. The whole channel was divided into about 50 bends (partial knees) and 20 diffuser sections of different cross-sections.

The mathematical model described (Table 3) was coded in FORTRAN by H. D. Hilbrich [5] in 1982.

For the cascade channel shown in Fig. 3, 15 streamlines Ψ and 11 planes in the half-space parallel to the side wall were chosen. The distances between these planes were kept small within the side wall boundary layer and larger in the centre of the channel.

For the numerical determination of the secondary flow field in the individual bends according to differential equation (1) in Table 3 a finite difference method was used. By means of the code mentioned above it is possible to compute the local secondary flow vorticity, the secondary flow stream function (Fig. 4), various characteristic parameters of the secondary flow field, as for instance the circulation and the vorticity centre coordinates, and the wall streamline field of the total flow resulting from the basic and secondary flows, Fig. 5 left. As the ideal secondary flow velocities are calculated in a sufficient number of equipotential surfaces by taking $\Phi = \text{const}$ (see Fig. 3) and $\Delta\Phi = 2$*) — the value and the direction of the total velocity can be determined following the superposition rule (see Fig. 6). An isoclinal field is obtained permitting to plot the streamlines shown in the left side of Fig. 5. The special features of the channel shown in Fig. 3 are the following:

for $\Phi < 0$, there are no fixed boundary walls,

for $\Phi = [0, 40]$, there is only one fixed boundary wall in flow direction, i.e. part of the blade profile surface and in case of

*) In the diffuser area $\Delta\Phi = 1$ was chosen.

$\Phi > 40$, there are two fixed boundary walls, i.e. the remaining parts of the pressure side *PS* and the suction side *SS* of the blade profile surface.

In case of unstable or open channel flow boundaries being kept constant, the set of 15 streamlines covered 4 or 3 channels, i.e. several adjacent channels had to be taken under consideration (see Fig. 3). Hence a relatively low supporting point density resulted in the weak secondary flow area and a relatively high supporting point density in the intense secondary flow area.

For the development of the electronic data processing program it proved to be advisable from the methodological point of view to determine simultaneously the secondary flow field by means of an electroanalogy model. This refers mainly to the supporting point arrangement selected and to FORTRAN program tests for which a reasonably accurate solution of equation (7) in Table 3, i.e. the electroanalogue solution, has been available.

4. Verification of the Theory

The same cascade channel (Fig. 3) was used by M. Rössler [11] to show experimentally the streamlines formed on the end and side walls by applying the soot/oil/petroleum method. Theoretical flow conditions in the channel inlet cross-section were in agreement with those observed experimentally.

In result of comparing the streamline patterns on the wall determined by means of the two methods demonstrated in Figs 5 left and right, the relatively simple mathematical model of the ideal secondary flow proved to be applicable. The comparison has been only a qualitative one as Fig. 5 left demonstrates the wall streamline field of a frictionless, i.e. modelled, flow while in Fig. 5 right the real flow field is shown. Boundary layers as indicated in Fig. 6 are not considered here although the collateral boundary layer has been used as secondary vorticity generator in equation (3) and (4) shown in Table 3. In the inlet area $\Phi = \text{const}$ (see Fig. 3) of the respective bend this collateral boundary layer generates the quasi-vortex tube ω_r shown in Fig. 2, which is, however, latent in the interior of the bend when lack of viscosity in the fluid is assumed.

Due to the relatively good correspondence between numerical and experimental results concerning the streamline pattern on the channel side wall formed in the inlet area of the curved channel (see Fig. 5), the wall streamline pattern was determined in the same way in the adjacent diffuser. As it is nearly rectilinear, the vorticity generation term at the right side of the differential equation (3) or the second term at the right side of equation (4) in Table 3 are not applicable. Consequently, the secondary flow field in the diffuser is only changed by the velocity ratio W (see: the left equation (5) in Table 3). The result of this investigation is shown in Fig. 7. In the centre, the streamline patterns formed on the channel side wall can be seen. In our case the main flow through the diffuser is frictionless and can be represented by means of equipotential surfaces. The diffuser begins at the equipotential surface $\Phi = 80$ and ends at $\Phi = 100$. In Fig. 7 the abscissa in the upper graphs represents the left (*PS*) edge of the diffuser channel (in flow direction) shown in the centre of the figure and

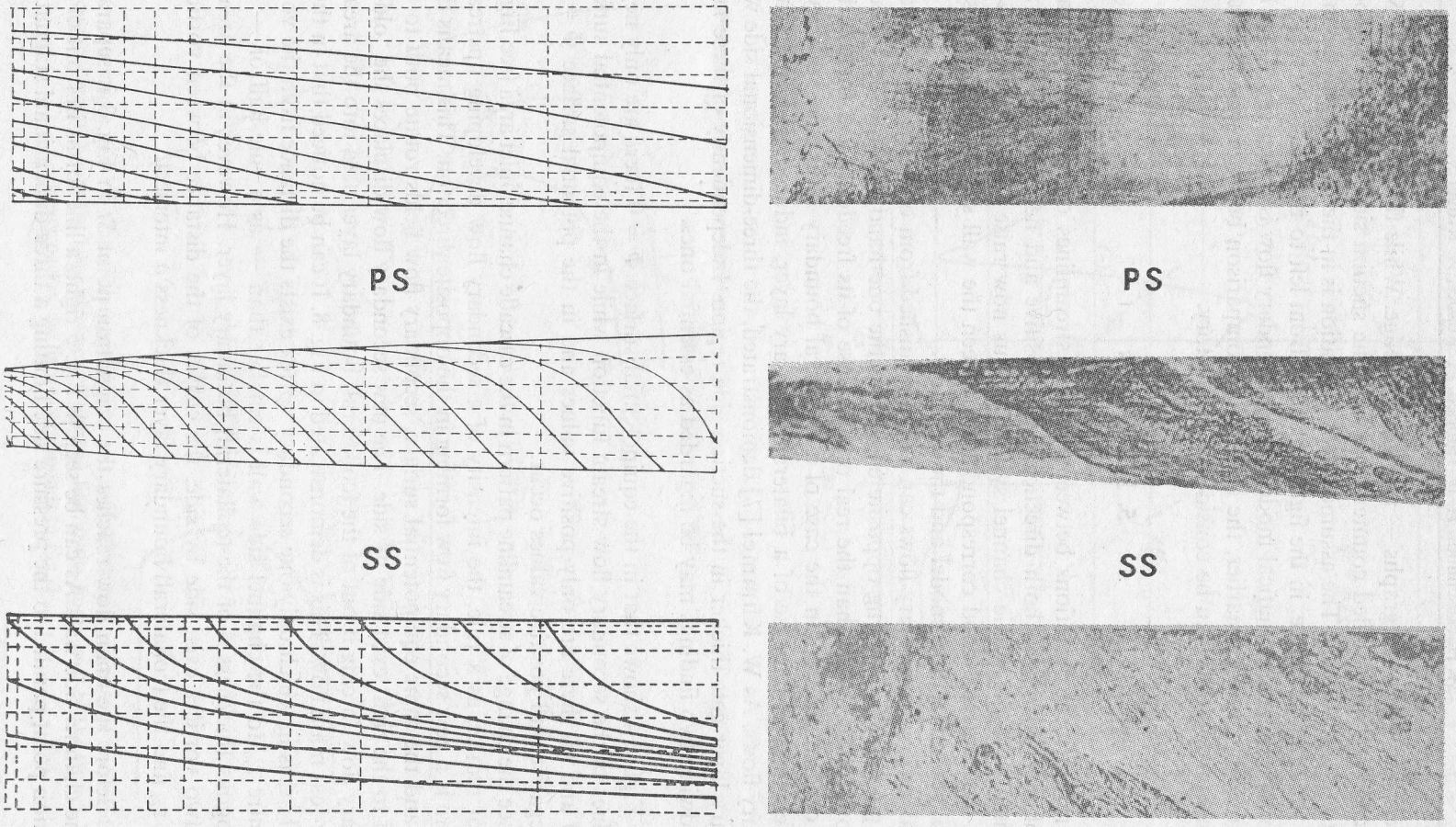

Fig. 7. Left: Wall streamline patterns determined numerically and describing the ideal vorticity-dependent flow in a diffuser with frictionless main flow (dashed lines: potential basic flow). Right: Respective wall streamline patterns made visible in an experimental way. Top: Pressure side *PS* of cascade channel. Centre: Channel side wall. Bottom: Suction side *SS* of cascade channel

the abscissa in the lower graphs — its right (*SS*) edge. While the pressure side *PS* of the cascade profile is folded counter-clockwise, the suction side *SS* is folded clockwise into the table plane. The assumed axis of rotation is in the direction of the main flow in the table plane, i.e. in the figure it shows from left to right.

Although our mathematical model of the secondary flow is rather simple, as has been already mentioned earlier, the qualitative comparison between numerical and experimental solutions can be considered satisfactory.

5. Main results

There are local deviations between the wall streamlines of the ideal fluid and those of the real one in both directions; but positive and negative deviations are distributed over the whole channel system. Let us now raise the question how to explain the relatively good correspondence between the wall streamline patterns of the ideal secondary flow model and the real flow.

Ideal and real secondary flows can be distinguished from one another by means of two phenomena showing opposite effects: on the one hand side the ideal secondary flow rotates faster than the real one because of its freedom from friction, but on the other hand side, in the case of a collateral boundary layer, less vorticity is generated than in the case of a bilateral boundary layer, induced by primary and secondary flows. As W. Kümmel [7] demonstrated, the three-dimensional side wall boundary layer gets thicker in the suction side region. Independently of these facts the following two findings may be regarded as essential ones.

5.1. Figure 4 shows that in the equipotential surface $\Phi = 0$ there are only negative values of the secondary flow stream function while in the equipotential surface $\Phi = 20$ and 40 there are only positive values and in the potential surface $\Phi = 10$ both negative and positive values occur.

Hence the change of streamline pattern in the cascade channel inlet area (see Fig. 3) does not reduce, as a rule, the intensity of a secondary flow developing upstream, but there is a new secondary flow forming in the opposite direction. This means that in one and the same equipotential surface, secondary flow fields rotate both to the left and to the right exist side by side. The new secondary flow displaces the "older" secondary flow forcing it out of the (collateral) boundary layer area into the area of the low-loss main flow. This is demonstrated in Fig. 8. It can be noticed that in those channel areas in which only one secondary vortex exists the distance from the vorticity centre z_ω to the channel side wall is smaller than — as a rule half of — the homologous thickness δ of the (collateral) boundary layer. However in the area in which two vortices exist side by side, the curves of the distance between vorticity centres z_ω and the (collateral) boundary layer thickness δ intersect.

5.2. Before the main flow reaches the stagnation point *St* in Fig. 3 it separates from the channel side wall. As can be seen in Fig. 5 right, a line forms in front of the stagnation point parallel to the pressure side limiting a three-dimensional stagnation

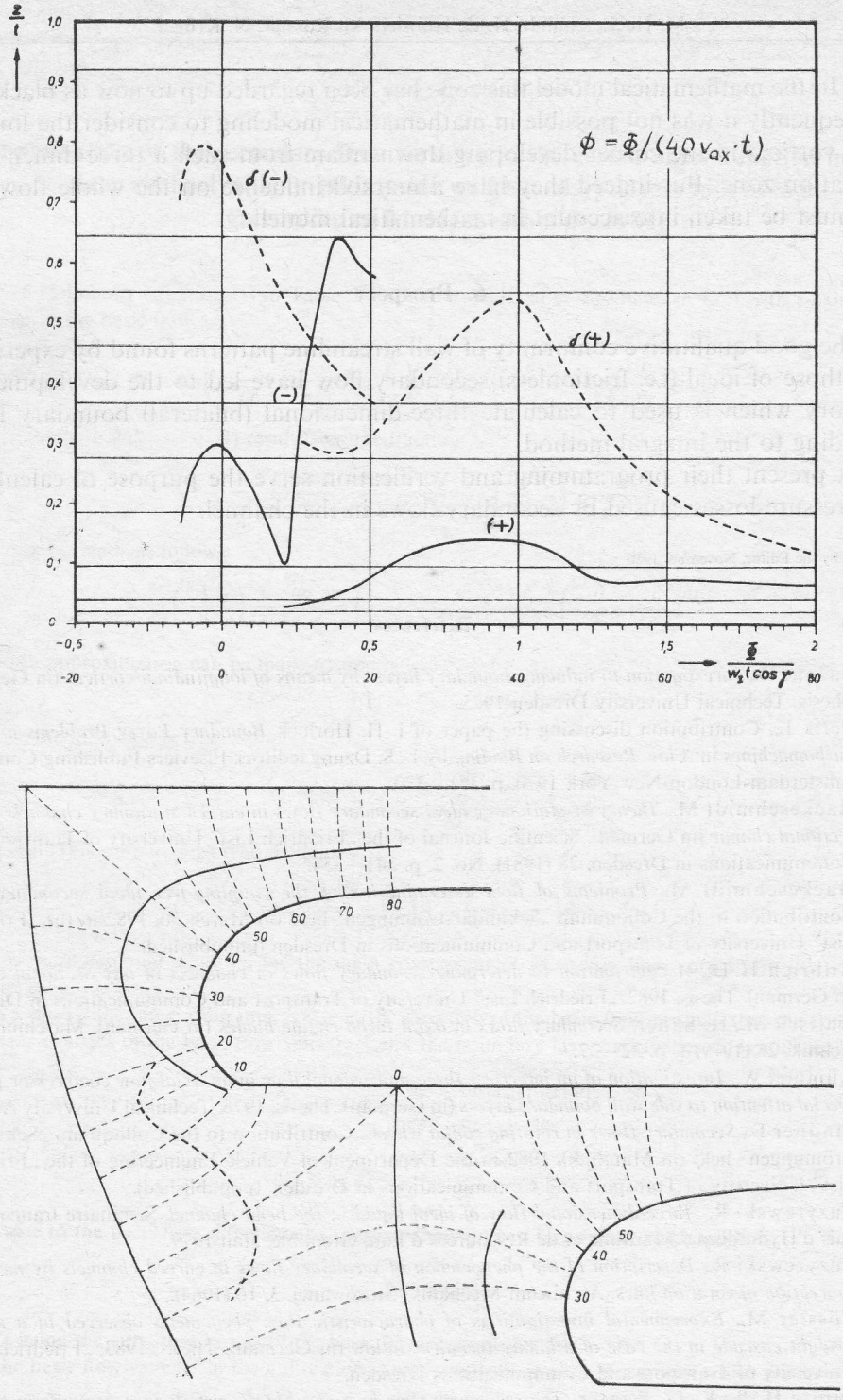

Fig. 8. Vorticity centre position of secondary vortices formed in an ideal fluid (continuous lines) and the homologous (collateral) boundary layer thickness δ (dashed line in the upper part of the figure). The lower part of the figure corresponds to Fig. 3

zone. In the mathematical model this zone has been regarded up to now as black-box. Consequently it was not possible in mathematical modeling to consider the longitudinal vortices in the corner developing downstream from such a three-dimensional stagnation zone. But indeed they have a marked influence on the whole flow field and must be taken into account in mathematical modeling.

6. Prospect

The good qualitative conformity of wall streamline patterns found by experiment with those of ideal (i.e. frictionless) secondary flow have led to the development of a theory which is used to calculate three-dimensional (bilateral) boundary layers according to the integral method.

At present their programming and verification serve the purpose of calculating the pressure losses caused by secondary flows in the channel.

Received by the Editor, November 1986

References

[1] Bažant D., *Investigation to influence boundary layers by means of longitudinal vortices* (in German). Thesis, Technical University Dresden 1975.

[2] Bělik L., Contribution discussing the paper of I. H. Horlock *Boundary Layer Problems in Axial Turbomachines* in: *Flow Research on Blading* by L. S. Dzung (editor): Elseviers Publishing Company, Amsterdam-London-New York 1970, p. 361—370.

[3] Hackeschmidt M., *Theory of stationary ideal secondary flows in curved stationary channels of any sectional change* (in German). Scientific Journal of the „Friedrich List" University of Transport and Communications in Dresden, 28 (1981), No. 2, p. 341—354.

[4] Hackeschmidt M., *Problems of field determination of the coupling-free ideal secondary flow.* Contribution to the Colloquium „Sekundärströmungen" held on March 30, 1982 in the „Friedrich List" University of Transport and Communications in Dresden (unpublished).

[5] Hilbrich H.-D., *A contribution to determine secondary flows in channels of any sectional change* (in German). Thesis, 1982, „Friedrich List" University of Transport and Communications in Dresden.

[6] Hultsch M., H. Sauer, *Secondary flows in axial turbo-engine blades* (in German). Maschinenbautechnik, 28 (1979) 1, p. 32—37.

[7] Kümmel W., *Investigation of an imperfect three-dimensional flow in an axial-flow compressor paying special attention to side wall boundary layers* (in German). Thesis, 1976, Technical University Aachen.

[8] Lindner E., *Secondary flows in rotating radial wheels.* Contribution to the Colloquium „Sekundärströmungen" held on March 30, 1982 in the Department of Vehicle Engineering of the „Friedrich List" University of Transport and Communications in Dresden (unpublished).

[9] Puzyrewski R., *Three-dimensional flow of ideal liquid in the bend channel.* Seminaire franco-polonais d'Hydraulique Maritime et de Ressources d'Eau, Grenoble, Juin 1979.

[10] Puzyrewski R., *Description of the phenomenon of secondary flows in curved channels by means of convection of rotation lines.* Archiwum Mechaniki Stosowanej, 3, 16 (1964).

[11] Rössler M., *Experimental investigations of characteristic flow phenomena observed in a special straight cascade in the case of a highly turbulent inflow* (in German). Thesis, 1983, „Friedrich List" University of Transport and Communications Dresden.

[12] Squire H. B., K. G. Winter, *The secondary flow in a cascade of airfoils in a nonuniform stream.* Journal of the Aeronautical Sciences, April 1951, p. 271—277.

[13] Wolf H., *Boundary losses in straight blade cascades* (in German). Thesis, 1960, Technical University Dresden.

Appendix

Determination of the secondary flow vorticity in the zeroth approximation in curved plane channel without taking side wall boundary layers into account (according to M. Hackeschmidt, 1981)

The Helmholtz equation (1) in Table 2 reads in cylindrical co-ordinates (r, ε, z) with z-axis directed parallel to the basic flow as:

$$\mathbf{e}_s = \mathbf{e}_\varepsilon : \left(\omega_r \frac{\partial}{\partial r} + \omega_\varepsilon \frac{1}{r}\frac{\partial}{\partial \varepsilon} + \omega_z \frac{\partial}{\partial z}\right)\frac{\tilde{v}+v'_\varepsilon}{r} = \left(v'_r \frac{\partial}{\partial r} + (\tilde{v}+v'_\varepsilon)\frac{1}{r}\frac{\partial}{\partial \varepsilon} + v'_z \frac{\partial}{\partial z}\right)\frac{\omega_\varepsilon}{r}. \tag{1}$$

The terms with $\partial/\partial\varepsilon$ in Eq. (1) result from the fraction:

$$\frac{\omega_\varepsilon}{r}\frac{\partial}{\partial \varepsilon}\frac{\tilde{v}+v'_\varepsilon}{r} - \frac{\tilde{v}+v'_\varepsilon}{r}\frac{\partial}{\partial \varepsilon}\frac{\omega_\varepsilon}{r} = -\left(\frac{\tilde{v}+v'_\varepsilon}{r}\right)^2 \frac{\partial}{\partial \varepsilon}\frac{\omega_\varepsilon}{\tilde{v}+v'_\varepsilon}. \tag{2}$$

Now Eq. (1) reads as follows:

$$\left(\frac{\tilde{v}+v'_\varepsilon}{r}\right)^2 \frac{\partial}{\partial \varepsilon}\frac{\omega_\varepsilon}{\tilde{v}+v'_\varepsilon} = \left(\omega_r \frac{\partial}{\partial r} + \omega_z \frac{\partial}{\partial z}\right)\frac{\tilde{v}+v'_\varepsilon}{r} - \left(v'_r \frac{\partial}{\partial r} + v'_z \frac{\partial}{\partial z}\right)\frac{\omega_\varepsilon}{r} \tag{3}$$

The 0-th approximation can be made assuming

$$v'_r = v'_\varepsilon = v'_z = \Phi, \tag{4}$$

whence the following is true:

$$\omega_\varepsilon = \omega_\varepsilon^{(\Phi)}, \quad 2\tilde{\omega}_r = \frac{1}{r}\frac{\partial r\tilde{v}}{\partial z}, \quad 2\tilde{\omega}_z = -\frac{1}{r}\frac{\partial r\tilde{v}}{\partial r}. \tag{5}$$

Equation (3) is simplified to read as follows:

$$\frac{\partial}{\partial \varepsilon}\frac{\omega_\varepsilon^{(\Phi)}}{\tilde{v}} = \left(\frac{r}{\tilde{v}}\right)^2 \left(\tilde{\omega}_r \frac{\partial}{\partial r} + \tilde{\omega}_z \frac{\partial}{\partial z}\right)\frac{\tilde{v}}{r}. \tag{6}$$

This is the differential equation for the main component of secondary flow vorticity in the zeroth approximation.

We choose the integration interval $\Delta\varepsilon$ in the direction of the basic flow so small that the confinement to linear changes of the basic flow velocity $\tilde{v}$ and the boundary layers vorticities $\tilde{\omega}_z$ is sufficient, whence

$$\tilde{v}(\varepsilon) = \tilde{v}(\Phi) = \frac{\partial \tilde{v}}{\partial \varepsilon}\varepsilon, \quad \frac{\partial \tilde{v}}{\partial \varepsilon} \frac{\tilde{v}(\Delta\varepsilon) - v(\Phi)}{\Delta\varepsilon}, \tag{7.1}$$

$$\tilde{\omega}(\varepsilon) = \tilde{\omega}(\Phi) + \frac{\partial \tilde{\omega}}{\partial \varepsilon}\varepsilon, \quad \frac{\partial \tilde{\omega}}{\partial \varepsilon} \frac{\tilde{\omega}(\Delta\varepsilon) - \tilde{\omega}(0)}{\Delta\varepsilon}. \tag{7.2}$$

Spanwise to the basic flow direction the rotation theorem can be applied which implies

$$\tilde{v}(r) \approx \tilde{v}(\tilde{r})\frac{\tilde{r}}{r}, \tag{8}$$

with $\tilde{r}$ being the curvature radius of the basic flow mean streamline.

The basic flow velocity in the z direction can be assumed to change stepwise which means

$$\frac{\partial \tilde{v}}{\partial z} \frac{\tilde{v}(\Delta z) - \tilde{v}(\Phi)}{z} \frac{\partial \tilde{v}}{\partial z}\Big|_{\frac{\Delta\varepsilon}{2}, \frac{\Delta z}{2}} \tag{9}$$

It follows from Eq. (8) that

$$\frac{\partial \tilde{v}}{\partial r\, r} = -\frac{2\tilde{v}(\tilde{r})}{\tilde{r}^2} \tag{10}$$

Thus the integral of the differential equation (6) is equivalent to equation (4) in Table 3.

Przepływy wtórne w kanałach zakrzywionych o dowolnej zmienności przekroju

Streszczenie

Celem wyznaczenia strat energetycznych wywołanych przepływami wtórnymi w zakrzywionych kanałach o dowolnej zmienności przekroju zastosowano model matematyczny stacjonarnego, nielepkiego (idealnego) pola przepływu. Jakościowa zgodność między wyznaczonymi numerycznie liniami prądu na ściankach specjalnie zakrzywionego kanału (program w języku FORTRAN) a liniami prądu wyznaczonymi doświadczalnie doprowadziła do opracowania metody obliczania trójwymiarowych warstw przyściennych. Przedstawiono podstawowe wyniki dotyczące zachowania się przepływów wtórnych w różnych warunkach.

Вторичные течения в искривлённых каналах произвольно переменного сечения

Резюме

Для определения энергетических потерь вызванных вторичными течениями в искривлённых каналах произвольно переменного сечения применяется математическая модель стационарного, невязкого (идеального) поля течения. Качественное согласие между номерически определёнными линиями тока на стенках специально искривлённого канала (программа на языке ФОРТРАН) и линиями тока экспериментально определёнными привело к разработке метода расчёта трёхразмерных пограничных слоев. Представлены основные результаты касающиеся поведения вторичных течений в различных условиях.